

## **Stereo PIV investigation of a round jet**

S. Grizzi<sup>1\*\*</sup>, M. Falchi<sup>1</sup>, G.P. Romano<sup>2</sup>

<sup>1</sup> Italian Ship Model Basin (INSEAN), Propulsion and Cavitation Unit; Via di Vallerano 139, 00128 Rome, ITALY

<sup>2</sup> University “La Sapienza”, Department of Mechanics and Aeronautics, Via Eudossiana 18, 00184 Rome, ITALY

### **1. ABSTRACT**

In the continuous effort of improving stereo PIV accuracy, particularly directed to the correct third velocity component evaluation, many different algorithms have been proposed: among the others, the one proposed by Soloff (Soloff et Al. 1997), based on stereoscopic vision principles, applies perspective calibrated functions on 2D velocity fields to obtain three velocity components accurate reconstruction.

The main aim of this work is to compare classical Soloff method with a new technique: image-dewarping method. This technique is based on the correction of the acquired images by using dewarping functions to apply a perspective deformation and reconstruct directly 3C velocity fields. To test the effectiveness of this technique in comparison to the Soloff one, an experimental investigation in the near field of a round jet has been performed; round jet is a well known, although not trivial, flow and a lot of theoretical and experimental data are available to make comparison.

### **2. Soloff and Image Dewarping Techniques**

By using a classical 2D-PIV technique, each displacement vector coming from the interrogation window contains both in-plane and out-of-plane component projection; to better estimate the in-plane components and to evaluate the third out-of-plane component, a simultaneous recording of images in a dual camera system can be used (Figure 1). In fact, using stereoscopic vision principles, the third component (orthogonal to laser sheet) of displacement can be obtained. Among the different methods, the Soloff one (Soloff et al. 1997) uses these principles to obtain 2D3C (two-Dimensional three-Component) vector field from a couple of 2D vector fields obtained from the cross-correlation of each frames couple of the two cameras. Image captured by stereoscopic rotational camera system are affected by distortions due to perspective. In general, the relationship between positions in the three-dimensional physical space of the flow,  $x$ , and the positions in the two-dimensional image recording plane,  $X$ , can be described by a nonlinear mapping function:

$$X = F(x) \tag{1}$$

---

\*\*  
s.grizzi@insean.it

**XIV AIVELA Annual Meeting  
Rome, 6-7 November 2006**

The information found by calibration can be used to do more than correct for distortion. Most PIV interrogation analyses determine the velocity vectors on a uniform grid fixed in the pixel array of the video camera, and the user has no ability to request data on a non-uniform grid in the fluid that may be more appropriate for the flow under consideration so mapping functions are usable to correct deformation. The use of a general mapping function found by calibration is very helpful in stereoscopic PIV because it eliminates the need to measure geometrical parameters of Stereo System, replacing them by mathematical mapping functions. In addition, the mathematics of the mapping function provide a natural framework in which to combine the images of two or more cameras to obtain the three-dimensional vector field.

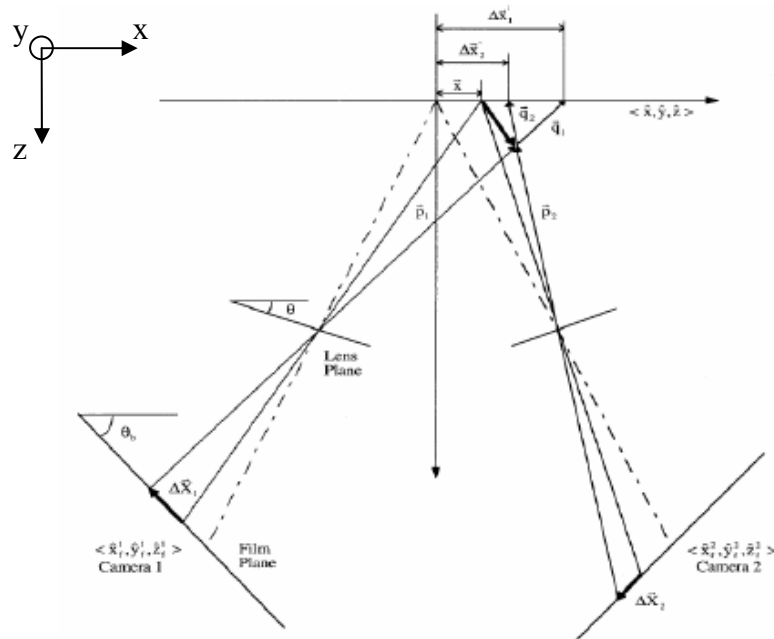


Figure 1: Displacement recorded by cameras affected by out of plane component in Rotational System (Zang & Prasad 1997)

Between exposures at times  $t$  and  $t + dt$  a particle at  $\mathbf{x}$  moves to  $\mathbf{x} + d\mathbf{x}$ . The displacement of its image is

$$\Delta X = F(\mathbf{x} + \Delta \mathbf{x}) - F(\mathbf{x}) \quad (2)$$

To first order the displacement is approximated by

$$\Delta X \approx \nabla F(\mathbf{x}) \Delta \mathbf{x} \quad (3)$$

**XIV AIVELA Annual Meeting  
Rome, 6-7 November 2006**

and the gradient

$$(\nabla F)_{i,j} = \frac{\partial F_i}{\partial x_j} \quad i=1,2 \text{ and } j=1,2,3 \quad (4)$$

Defining a ROI (Region of Interest) and a grid inside, it is possible to transform ROI grid into image coordinates (Figure 2) and interpolate velocity in these points from vectors obtained by a cross-correlation algorithm on a rectangular grid.

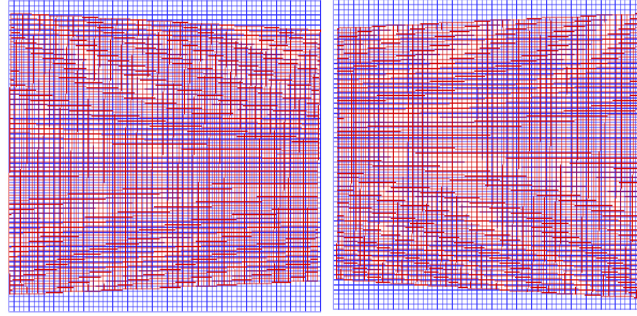


Figure 2: Overlap of Trasformed Left and Right ROI (in Red) to cross-correlation grid (in blue)

Due to the reduced light sheet thickness, it is possible to assume  $x_3=0$  in eq. (3), writing for the ROI points of 2 camera stereo system (where  $\Delta X^{(n)}$  are known n-camera displacements and  $\Delta x$  are searched displacements):

$$\begin{pmatrix} \Delta X_1^{(1)} \\ \Delta X_2^{(1)} \\ \Delta X_1^{(2)} \\ \Delta X_2^{(2)} \end{pmatrix} = \begin{pmatrix} F_{1,1}^{(1)} & F_{1,2}^{(1)} & F_{1,3}^{(1)} \\ F_{2,1}^{(1)} & F_{2,2}^{(1)} & F_{2,3}^{(1)} \\ F_{1,1}^{(2)} & F_{1,2}^{(2)} & F_{1,3}^{(2)} \\ F_{2,1}^{(2)} & F_{2,2}^{(2)} & F_{2,3}^{(2)} \end{pmatrix} \begin{pmatrix} \Delta x_1 \\ \Delta x_2 \\ \Delta x_3 \end{pmatrix} \quad (5)$$

Although it appears that the system in (5) is overdetermined, the second and fourth equations are linearly dependent. For example, adding the two dependent equations, a well-determined solvable system is obtained. In this way it is easy to solve system in (5) obtaining a 2D3C vector field. As a mapping function, a third-degree polinomial function can be used for x and y variables, a second order for z (Soloff et al. 1997) is sufficient.

$$\begin{aligned} X^j = & a_0 + a_1x + a_2y + a_3z + a_4x^2 + a_5xy + a_6y^2 + a_7xz + a_8yz + a_9z^2 + a_{10}x^3 \\ & + a_{11}x^2y + a_{12}xy^2 + a_{13}y^3 + a_{14}x^2z + a_{15}xyz + a_{16}y^2z + a_{17}xz^2 + a_{18}yz^2 \end{aligned} \quad (6)$$

**XIV AIVELA Annual Meeting  
Rome, 6-7 November 2006**

The coefficients in (6) are easy to be calculated using a least-square method from the acquired calibration target coordinates at different  $z$  planes close to the  $z=0$  position (where  $z=0$  is approximately the laser sheet position). No enhancement of the solution accuracy is attained increasing further the polynomial order (Willert 1997); in fact representing the position calibration errors for the two and three degree polinomial mapping functions (Figure 3), they are condensed around 0 following a Gaussian trend with a lower variance for third order one.

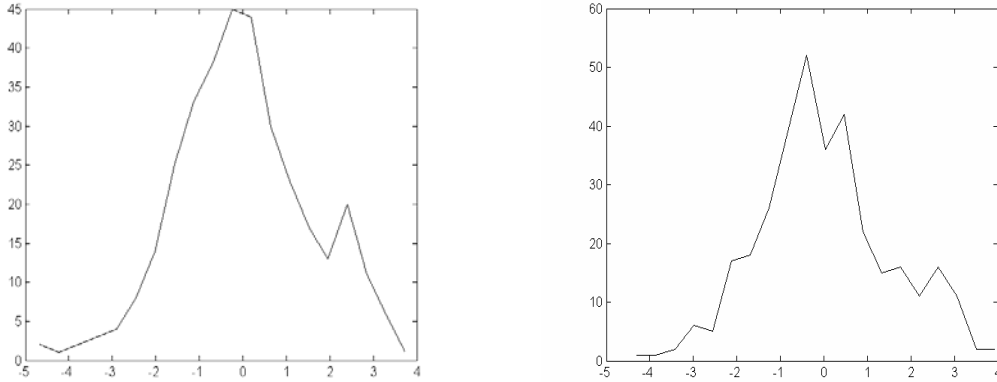


Figure 3: Second (left) and third (right) order polinomial error

Soloff method is the quickest and more diffused method but is affected by interpolation errors; it also smoothes the spatial gradients because of its dependence on the four interrogation windows vectors around (Figure 4). So in the case of a  $64 \times 64$  px interrogation window, with a 50% overlap, the final vector is influenced at least by a  $96 \times 96$  px window. Another disadvantage is the different interrogation window resolution through image.

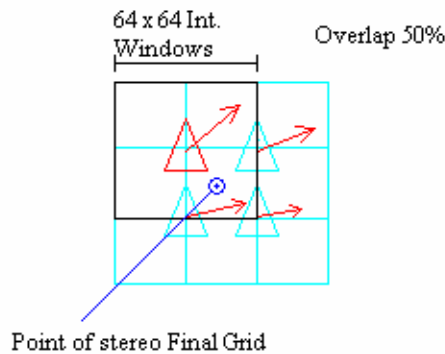


Figure 4: Dependence of interpolated point on a expanded interrogation window.

**XIV AIVELA Annual Meeting  
Rome, 6-7 November 2006**

To avoid these problems still using standard cross-correlation algorithms, a new Image Dewarping technique (Coudert et al. 2001) is introduced in present work. Usually image dewarping is used to evaluate misalignment between calibration target and laser sheet; in this case, mapping functions are applied on images sample to correct perspective and disparity maps on dewarped frames are used to correct misalignment. Another use of dewarping is possible applying it to all frames to correct perspective and to eliminate out of ROI (Figure 5). In this way, images coming from the two cameras have the same spatial resolution so, using standard cross-correlation algorithms over corrected images, resultant vector fields are evaluated on the same points. Having velocity information over coincident grids, a direct 3C reconstructions is possible to (7), without interpolation errors and decreasing spatial gradients smoothing. Unfortunately dewarping method makes unusable the gradient matrix  $F_{i,j}$  because erase perspective informations from images transforming it into frames captured by a translational system from infinite distance. (Figure 6)

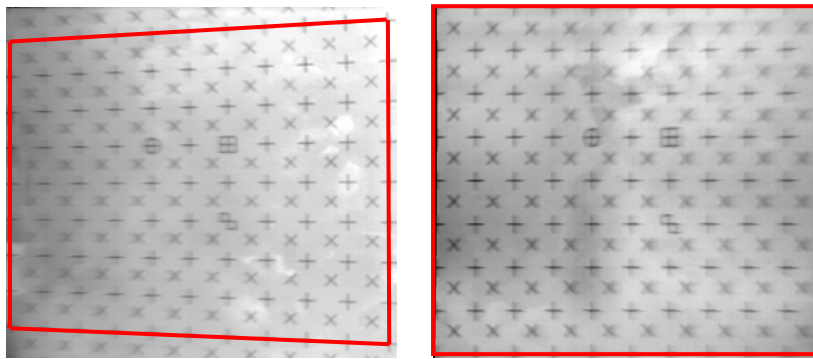


Figure 5: Dewarping of a calibration image and cutting of Out of ROI zone (ROI in red).

$$u = \frac{U_1 + U_2}{2}$$

$$v = \frac{V_1 + V_2}{2}$$

$$w = \frac{U_1 - U_2}{2 \tan \beta}$$

(7)

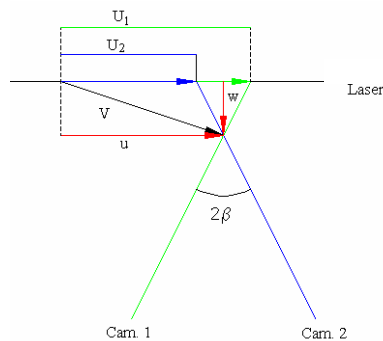


Figure 6: Sketch of direct reconstruction.

**XIV AIVELA Annual Meeting**  
**Rome, 6-7 November 2006**

The use of direct reconstruction equations (7) makes the knowledge of stereo system geometrical properties, e.g. the camera-laser sheet angle, necessary. To dewarp images it is necessary to calibrate a mapping function similar to (6) using the same least-square method. (Flow chart in Figure 7)

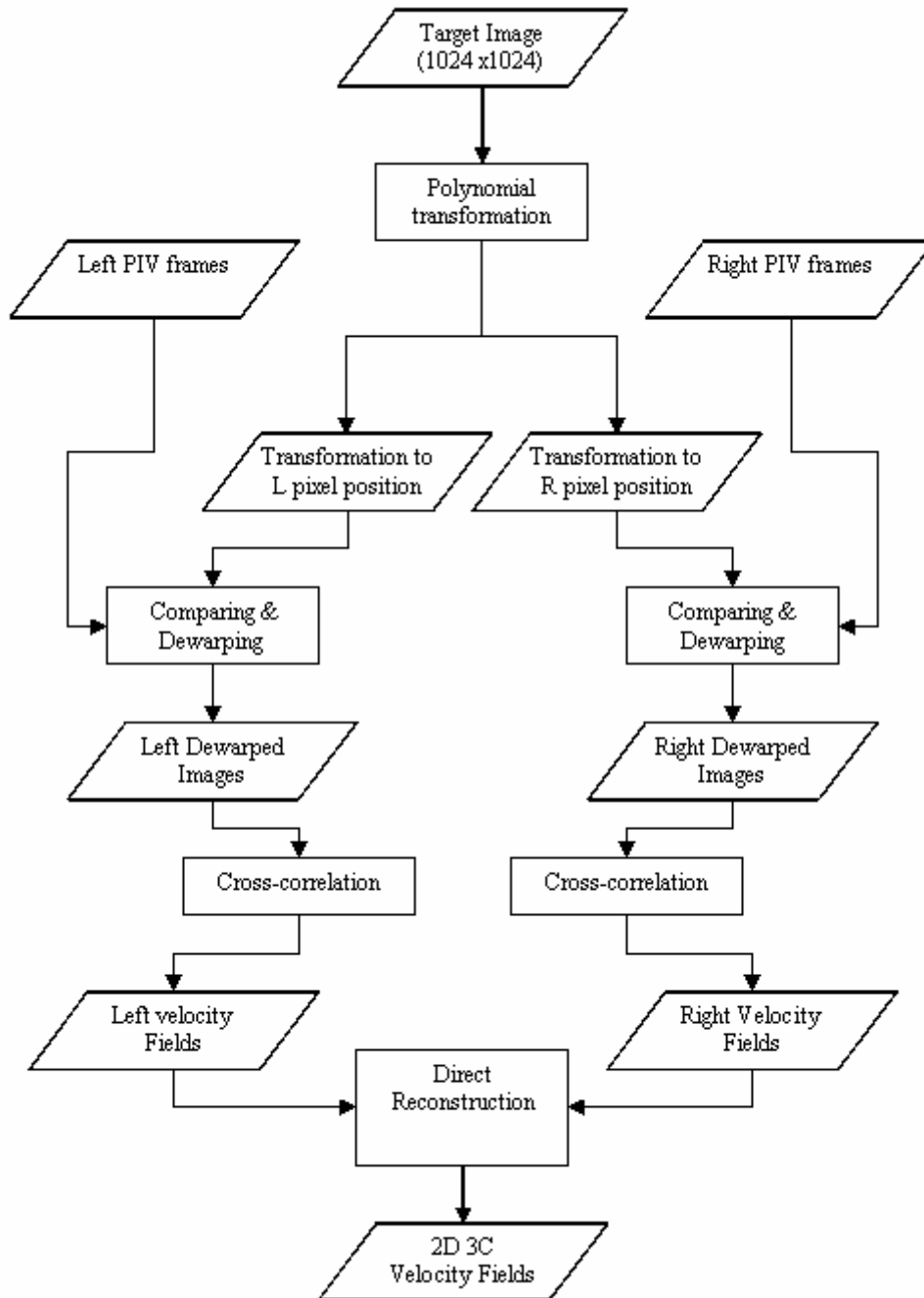


Figure 7: Flow chart for Image Dewarping.

## XIV AIVELA Annual Meeting Rome, 6-7 November 2006

Then, applying functions to pixel coordinate, images are dewarped. Being pixel coordinate represented by integer values and the transformation gives real values, a near pixel filter is used, approximating real values to near integers. Dewarped images are then analyzed by a cross-correlation algorithm and velocity fields are extracted with direct reconstruction equations without interpolation. As a first comparison, the computational cost of the different approaches has been evaluated on 100 images sets. (Figure 8)

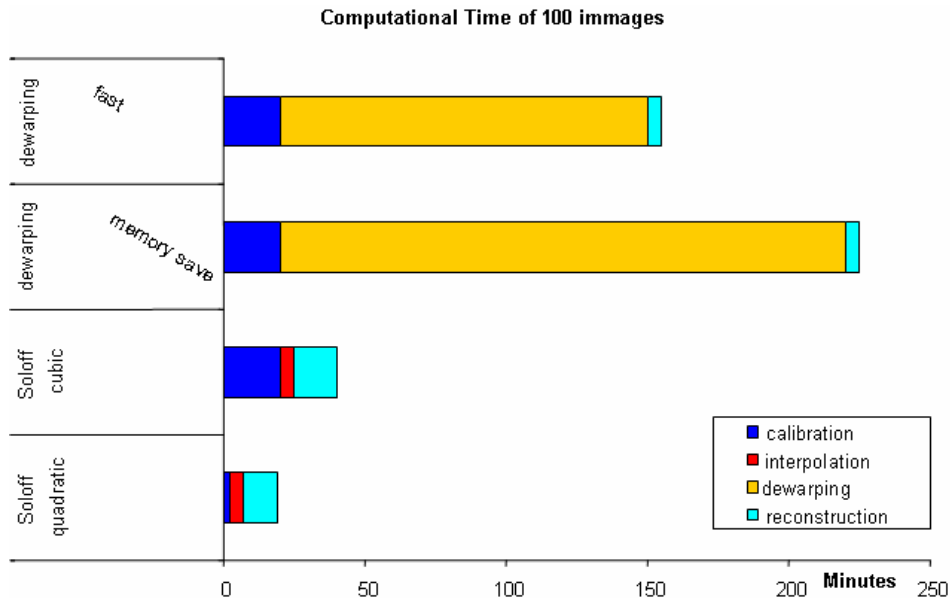


Figure 8: Computational Cost.

Two Image dewarping algorithms are compared; these programs use PC memory in different ways: first to safe time, second to safe memory. It is clear as the Soloff method has a very low computational cost (five-time lower than the dewarping methods) using the same degree of mapping function (cubic Soloff vs Cubic Dewarping); this is quite trivial because Soloff method works on grid nodes only while Dewarping one on all pixels. Moreover, dewarping technique introduces other problems as lower dewarped image quality that brings more spurious vectors in the evaluated fields where vector validation in post processing has been used.

### 3. ROUND JET

To compare Dewarping tecnique with Soloff one, an experimental campaign in near field of a round jet was performed. Round jet is a well known flow and a lot of experimental and numerical data are available to make comparisons.

When a circular jet enter in a stagnant fluid creates a conic zone of steady flow (potential core) extended to an axial distance of 3-5 D (where D is the outlet jet diameter) (Rajaratnam 1976). Beyond this distance, the turbulence produced by the shearlayers reaches jet centreline changing velocity profiles and creating a fully developed flow zone. (Figure 9)

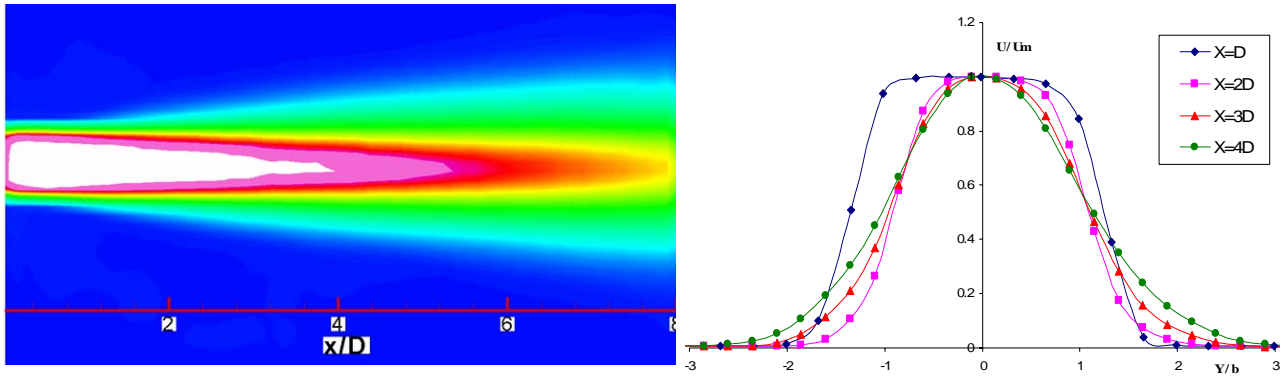


Figure 9: On the left extension of Potential core (white), on the right development of potential core velocity profiles.

Defining  $U_0$  as entry jet speed,  $U_m$  as local top axial speed,  $b$  as radial distance where local speed is half of top speed, jet self-similarity of non-dimensional axial velocity profiles is observed by Trupel\* 1926. A lot of data are available about jet self-similarity profiles (for instance axial, vertical speed and Reynolds stress profiles); empirical solutions are also available such as Tolmien, Goertler type (Rajaratnam 1976) and Integral solution (Agrawal e Prasad 2003). It is also evaluated axial jet decrease that follow linear profile out of potential core

$$U_0 / U_m = x / C \cdot D \quad (8)$$

Many different evaluation of the  $C$  coefficient are available in literature (for instance: Trupel\* 1926, Hinze and Zijnen\* 1949).

#### 4. EXPERIMENTAL SETUP

To generate the round jet, a hydrodynamic tunnel, presented in Figure n. 10, has been used; a constant level tank with honeycomb screens is connected by a first convergent (Aspect ratio 15:1) to a duct, a second convergent (Aspect ratio 50:1) and finally to the test chamber. This chamber has square section 46 cm wide and 96 cm long. Operative range extends from  $Re = 10^3$  to  $10^6$ . Nozzle diameter ( $D$ ) is 2 cm wide.

An infrared diode laser (emission wavelength  $\lambda = 800$  nm) has been used to generate light sheet (Max Power 42W). Hollow glass spheres, with density similar to the water (diameter 10  $\mu$ m) has been used as seeding particles. Two Photron Fastcam-Ultima APX high speed cameras, capable to acquire 2000 frames per second at the maximum resolution of 1024x1024 pixels, have been used to acquire PIV frames. Two Nikon AF Nikkor 50 mm objectives have been mounted on the two cameras. A classical forward-forward stereo-optical configuration with half visual angle of 45° and 5° Sheimpflug angle has been used (Figure 10); as calibration target, a dual plane one (3D) made of a glass plate (1.5 mm thick) with dot's grids (10 mm mesh) on both sides has been set to calibrate the stereo system.

**XIV AIVELA Annual Meeting  
Rome, 6-7 November 2006**

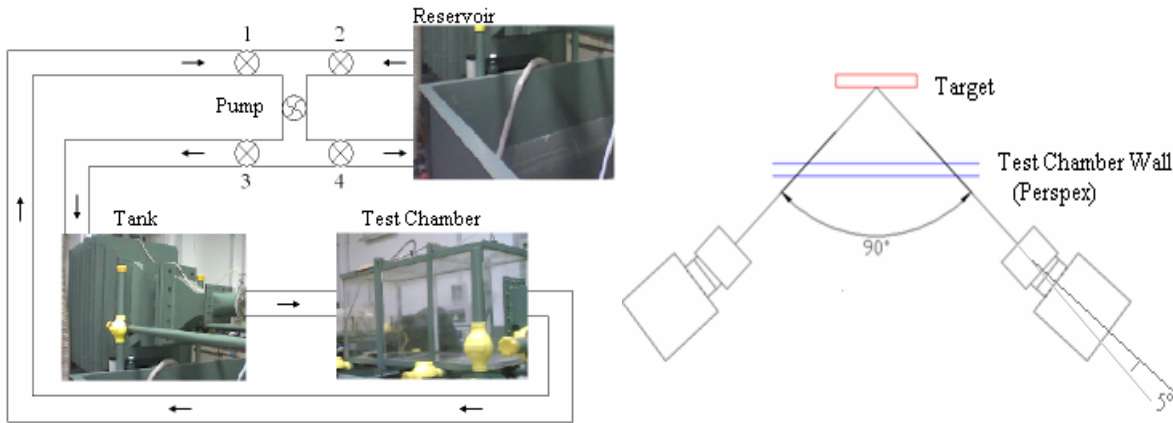


Figure 10: Hydrodynamic Tunnel Scheme (right) and stereo rotational system (left).

A first experimental campaign, to study the particular features of the used apparatus, using a classical 2D PIV system has been performed, followed by a second experimental phase using Stereo-PIV; the tested Reynolds number was equal to 15000, thus fully turbulent.

### 5. TEST RESULTS

To accomplish experimental campaigns, the cameras frame rate was set to 2000 fps, to have sufficient particle illumination level and to avoid excessive speed elongation of particles images. A 20000 frames set, selected from different acquisitions, were analyzed with a standard cross-correlation based software (PIVMAR developed at the Mechanics and Aeronautics Department of University of Rome “La Sapienza”). Capture and correlation parameters are resumed in Figure 11. To make a comparison between methods and literature data, some characteristics of analyzed circular jet are reported as inverse axial velocity decrease ( $U_0/U_m$ ), (Figure 12), self similarity of non-dimensional axial and vertical velocity profiles (Figure 13), third component of velocity (Figure 14) and Reynolds stress profiles (Figure 15) evaluated at 8 diameters from jet nozzle. As resumed in the next table the different values for C coefficient of the axial velocity component decrease are close to the literature ones.

|                          |      |
|--------------------------|------|
| Trupel (1926)*           | 7.32 |
| Hinze e Zijnen (1949)*   | 6.39 |
| Albertson et al. (1950)* | 6.3  |
| Stereo PIV Soloff (Q)    | 7.58 |
| Stereo PIV Soloff (C)    | 7.47 |
| Stereo PIV Dewarping     | 7.48 |

**XIV AIVELA Annual Meeting  
Rome, 6-7 November 2006**

|                                      |                              |                               |      |
|--------------------------------------|------------------------------|-------------------------------|------|
| Magnification factor                 | 1 px/mm                      | Max iteration discrete offset | 7    |
| Time delay                           | 500 $\mu$ s                  | Validation iteration number   | 3    |
|                                      | Max - Min                    | Initial tolerance             | 4 px |
| Interrogation Windows                | 128 x 128 px<br>- 64 x 64 px | Final tolerance               | 2 px |
| Offset Subpixel                      | Yes                          | Substitution filter           | D    |
| Max iterations number<br>offs. Subp. | 5                            | Min numb. vect. mean<br>calc. | 2    |
| Grid node distance                   | 16 px - 75%                  |                               |      |

Figure 11: Capture and correlation parameters.

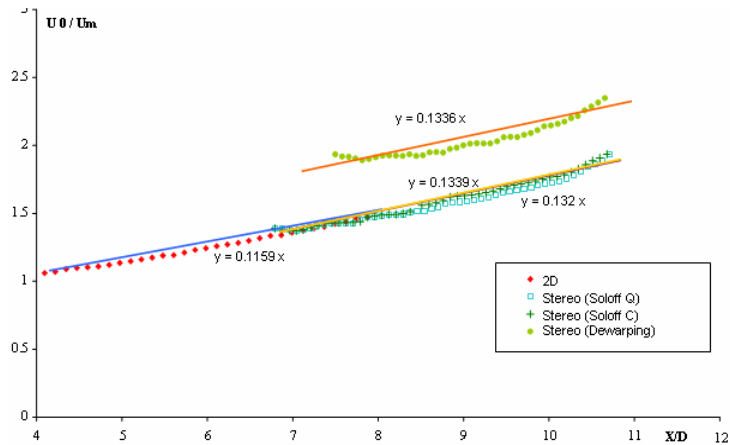


Figure 12: inverse axial velocity decrease ( $U_0/U_m$ )

It is evident in Figure 12 how the decrease agrees with PIV 2D campaign; in Dewarping Technique outliers are present as visible imperfections in peripheral zone because of the presence of the perspex wall introducing reflections and bad images quality. Dewarping algorithm is very sensible to low quality zones: by reducing perspective deformations, it expands overmuch or deletes particles from corrected frames particularly where image quality is low.

In Figure 13 self-similarity of velocity profiles are presented; axial velocity profiles follow both PIV 2D and theoretical solutions - Tollmien and Goertler solutions. Radial velocity evaluated by stereo methods follow theoretical curves better than PIV 2D principally because this velocity component is calculated with a mean value between two fields, decreasing errors of common PIV.

In Figure 14, azimuthal (third component) profile highlights the presence of a strong out-of-plane rotational component probably caused by troubles in honeycomb of first convergent, as confirmed by a cross-section 2D PIV study (Figure 14).

It is also evident how Dewarp method presents no imperfections in third component velocity profile usually given by interpolation errors.

Figure 15 makes evident as Reynolds stresses are less smoothed by Dewarping method in respect to Soloff one; anyway, it isn't possible to make comparisons with literature data because the analyzed jet zone is far from fully developed self

**XIV AIVELA Annual Meeting  
Rome, 6-7 November 2006**

similarity zones (starting at  $x/D= 20$  , Weisgraber & Liepmann 1998, Webster et al. 2001) and the presence of transversal rotating velocity profile (Figure 14) changes self similarity of second order variables.

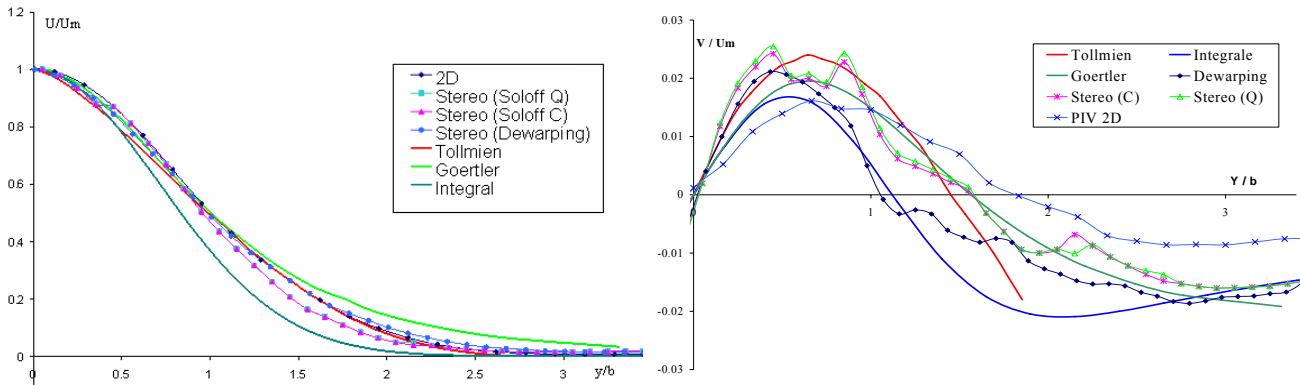


Figure 13: Non-dimensional axial velocity ( $U/U_0$ ) (up) and Vertical velocity ( $V/U_0$ ) (down) profiles.

**6. CONCLUSIONS**

PIV methods are usually a compromise between accuracy and computational cost; in fact a lot of experimental campaigns need so a large quantity of frames to make not possible to use a slow algorithm. The Soloff method well known defects can be avoided by enhancing interpolation algorithms; by doing so the enhanced capabilities, low computational cost and good accuracy, make it the most used method in SPIV programs. Image Dewarping avoids interpolation errors, gives less smoothed results and makes uniform spatial resolution in interrogation windows; on the other hand its high computational cost makes it unusable when a lot of images have to be analyzed. Moreover, the tendency to decrease the images quality can introduce errors in vectors evaluating when using cross-correlation algorithms. Possible enhancements have to use advanced image-treatment functions to speed up the evaluation and to increase dewarped images quality.

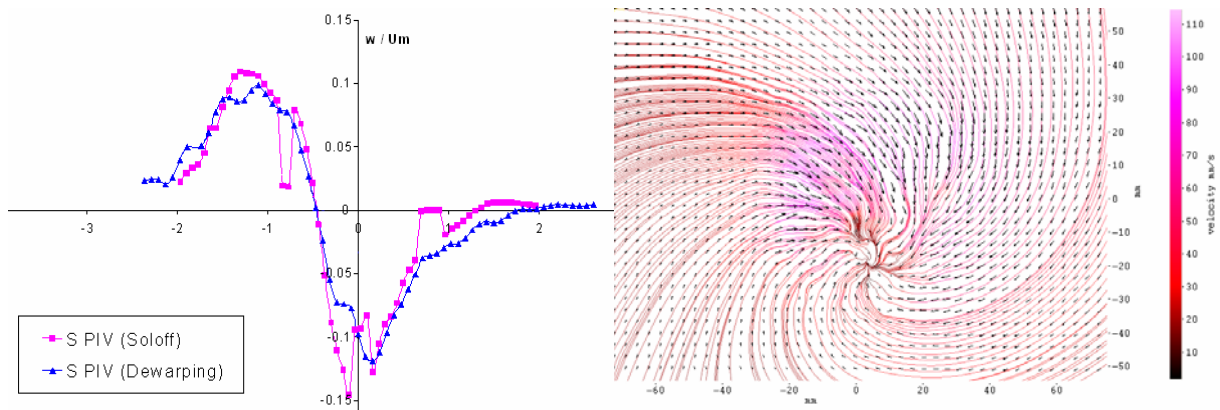


Figure 14: Non-dimensional transversal profile and streamlines from a transversal PIV study.

**XIV AIVELA Annual Meeting  
Rome, 6-7 November 2006**

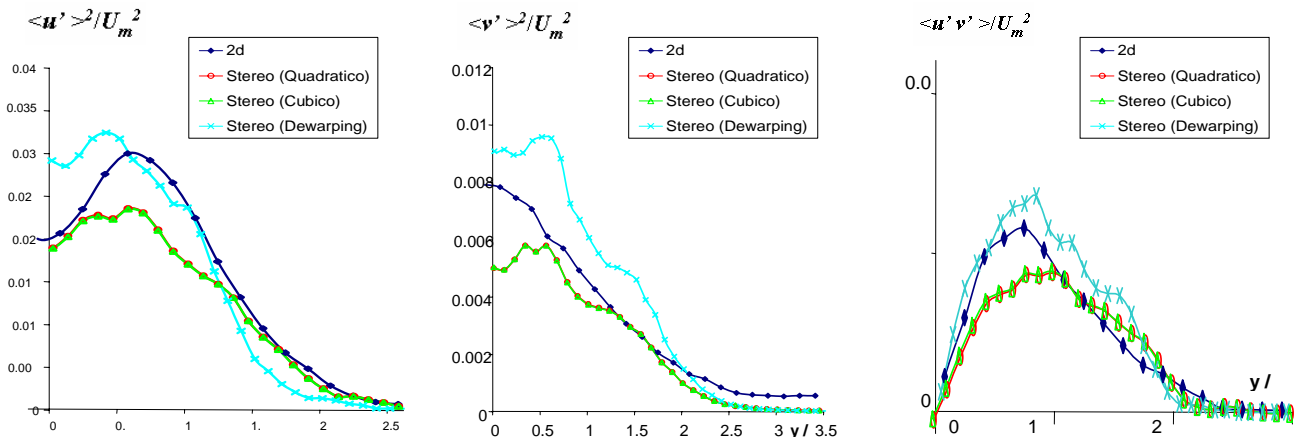


Figure 15: Comparing between Reynolds stress

**References \***

- Adrian R. J. "Twenty years of particle image velocimetry", *Experiments in Fluids* **39**, 159 – 169 , 2005
- Agrawal A., Prasad A. K "Integral Solution for the Mean Flow Profiles of Turbulent Jets, Plumes, and Wakes", *Journal of Fluids Engineering* **125**, 813 – 822 , 2003
- Cenedese A., Doglia G., Romano G. P., De Michele G., Tanzini G. "LDA and PIV Velocity Measurements in Free Jets", *Experimental and Thermal Fluid Science* **9**, 125 – 134 , 1994
- Coudert S.J.M. and Schon J.P. "Back-projection algorithm with misalignment corrections for 2D3C stereoscopic PIV", *Meas. Sci. Technol.* **12**, 1371 – 1381, 2001
- Hussein H. J., Capp S. P. e George W. K. "Velocity measurements in a high-Reynolds-number, momentum-conserving, axisymmetric, turbulent jet", *Journal of Fluid Mech.* **258**, 31 – 75 , 1994
- Prasad A. K., Adrian R. J. "Stereoscopic particle image velocimetry applied to liquid flows", *Experiments in fluids* **15**, 49 – 60 , 1993
- Rajaratnam N. *Turbulent Jets*, Elsevier Publishing Co., Amsterdam and New York, 1976
- Soloff S. M., Adrian R. J. e Liu Z. C. "Distortion compensation for generalized stereoscopic particle image velocimetry", *Meas. Sci. Technol.* **8**, 1441 – 1454 , 1997
- Webster D. R., Roberts P. J. W. e Ra'ad L. "Simultaneous DPTV/PLIF measurements of a turbulent jet", *Experiments in Fluids* **30**, 65 – 72 , 2001
- Weisgraber T. H., Liepmann D. "Turbulent structure during transition to self-similarity in a round jet", *Experiments in Fluids* **24**, 210 – 224 , 1998
- Zang W., Prasad A. K. "Performance evaluation of a Scheimpflug stereocamera for particle image velocimetry", *Applied Optics* **36**, n°33, 8738 – 8744 , 1997

---

\* Trupel observations (1926), Hinze and Zijnen (1949), Albertson et al. (1950), Willert (1997) data were obtained from publications in references.